Journal of Cultural Heritage 55 (2022) 158–170

Contents lists available at ScienceDirect

Journal of Cultural Heritage

journal homepage: www.elsevier.com/locate/culher

Original article

Corrosion phenomena and patina on archaeological low-tin wrought bronzes: New data

Panagiota Manti[a,*], David Watkinson[b]

[a] Department of Environment, Ionian University, Zakynthos, Panagoula, 29100, Greece
[b] Department of Archaeology and Conservation, Cardiff University, Humanities Building, Colum Drive, CF24 4EU, Cardiff, UK

ARTICLE INFO

Article history:
Received 8 July 2021
Accepted 9 March 2022
Available online 28 March 2022

Keywords:
Archaeological bronze corrosion
Low-tin bronze
Bronze corrosion
Cultural heritage materials

ABSTRACT

The study reports a systematic examination and analysis of low-tin wrought bronzes from archaeological burial environments in the Mediterranean. The corrosion profiles occurring on samples taken from thirty-six predominantly Corinthian and Illyrian helmets from excavations in Greece, were analysed using polarised metallography, SEM-imaging, SEM-EDX and X-Ray Diffraction methods. Analysis confirms and expands understanding of existing corrosion models for copper dissolution producing smooth tin enriched patinas that preserve the original surface as a marker layer. SEM-EDX compositional analysis of corrosion profiles with complementary imaging is used to discuss the conditions in which certain corrosion profiles are formed. The study reveals how analysis of samples from many objects of a similar manufacture, buried for similar time periods, can be used to develop detailed understanding of corrosion processes and provide better understanding of the likely appearance of the objects in antiquity.

Introduction

Study and analysis of the surface of archaeological bronzes and their corrosion profiles is important for developing understanding of the original appearance of objects in antiquity and their production technology, as well as for identifying forgeries [1,2] (p. 349). Bronzes may have been coloured by artificial patination, whereby a corrosion layer is deliberately formed to provide colouration that includes blue, green, red, yellow, black [3]. Understanding of corrosion mechanisms of bronzes developed during their burial is fundamental for understanding what comprises evidence of natural or intentional patination, plating, or other surface 'finishing patinas'.

Research aim

This work aims to advance understanding of corrosion and patina formation on archaeological low-tin bronzes (i.e. Cu-Sn alloys with tin content below 14 wt%) during their burial and to consider how the patina offers insight into the original appearance of an object. The paper (i) provides a sample set from objects of similar composition and manufacture, by collecting samples from 36 Greek low-tin wrought bronze helmets from a range of excavations in Greece; (ii) records the appearance and composition of corrosion profiles of the samples using polarised metallography, SEM-imaging, SEM-EDX and X-Ray Diffraction methods; (iii) uses the data collected to discuss the development of corrosion on the helmets.

Theory

Original appearance of objects

The concept of 'patina' goes back to the perceptions of art historians, predominantly in the Renaissance period, when it was believed that classical bronzes were originally deliberately patinated black and because of this, in later periods organic coatings were applied on bronzes to darken their appearance [2] (p. 353). In the context of archaeological conservation, the term 'patina' is not strictly defined but is broadly associated with the presence of a corrosion layer that marks the original surface [4]. Archaeological bronzes may acquire a 'patina' of corrosion during burial and its origins may be difficult to identify, as there are the extrinsic factors of the burial environment variables to consider and intrinsic factors within the object such as composition, manufacture and surface finishing processes. A 'fine' patina can provide information on polishing and other surface finishing techniques.

* Corresponding author.
E-mail addresses: pmanti@ionio.gr (P. Manti), watkinson@cf.ac.uk (D. Watkinson).

https://doi.org/10.1016/j.culher.2022.03.004
1296-2074/

Table 1
Details of helmet samples and their position on helmets.

Helmet Code	Excavation	Acc. No.	Type	Sample Code	Sample Position on Object
Archaeological Museum of Olympia, GR					
OL11	Olympia	B7170	Illyrian	OL11.1	cheekpiece, right, middle
OL13	Olympia	BE58	Illyrian	OL13.1	cheekpiece, right, low part
OL17	Olympia	ab34	Corinthian	OL17.1	cheekpiece, right, middle
OL21	Olympia	ab64	Corinthian	OL21.1	neckguard, lower part
OL27	Olympia	B9805	Corinthian	OL27.1	side
OL29	Olympia	B2608	Corinthian	OL29.1	crown, top
OL31	Olympia	B2648	Corinthian	OL31.1	crown
OL4	Olympia	B3348	Illyrian	OL4.2	crown, top
OL41	Olympia	B10534	Corinthian	OL41.1	cheekpiece, right
OL44	Olympia	B7073	Corinthian	OL44.1	neckguard, left
OL46	Olympia	B1501	Corinthian	OL46.1	neckguard, top
OL49	Olympia	B4411	Corinthian	OL49.1	crown, rear
OL5	Olympia	B4821	Illyrian	OL5.1	crown, upper left
OL50	Olympia	B4698	Corinthian	OL50.1	crown, rear
OL53	Olympia	B6550	Corinthian	OL53.1	neckguard, upper left
OL57	Olympia	B10526	Corinthian	OL57.1	unknown, loose fragment
OL58	Olympia	B10528	Corinthian	OL58.1	unknown, loose fragment
OL63	Olympia	B5177	Corinthian	OL63.1	unknown, loose fragment
OL66	Olympia	B7080	Chalkidian	OL66.2	crown, middle back
OL69	Olympia	B10527	Corinthian	OL69.1	crown, top, by the high ridge
OL70	Olympia	B4799	Corinthian	OL70.1	crown, middle back
OL71	Olympia	B5070	Corinthian	OL71.1	side, right
OL73	Olympia	B5167	Corinthian	OL73.1	neckguard, upper
OL74	Olympia	B5176	Corinthian	OL74.1	unknown, loose fragment
OL75	Olympia	B5178	Corinthian	OL75.2	crown
OL78	Olympia	B4667	Illyrian	OL78.1	crown, front, lower
OL79	Olympia	B5239	Chalkidian	OL79.1	unknown, loose fragment
OL9	Olympia	B5115	Illyrian	OL9.2	crest-track, left ridge, back
Archaeological Museum of Pella, GR					
PE1	Archontiko	A2001G10	Illyrian	PE1.1	crest-track, high ridge
PE2	Archontiko	A2002G194	Illyrian	PE2.2	crest-track, middle small ridge
PE3	Archontiko	A2001G9	Illyrian	PE3.1	crown, top, by the high ridge
PE4	Archontiko	A2002G189	Attic	PE4.3	neckguard, upper
Archaeological Museum of Thessaloniki, GR					
AP4	Aghia Paraskevi	MΘ16405	Illyrian	AP4.2	crest-track, high ridge
AP5	Aghia Paraskevi	MΘ16423	Illyrian	AP5.1	neckguard, lower part
Pitt Rivers Museum, UK					
PR1	Unknown	1884.32.16	Corinthian	PR1.1	crown, front
PR4	Unknown	1884.32.15	Etruscan	PR4.1	side, lower

Polychromy in Greek antiquity and on later metals is discussed elsewhere [1,3,5]. Other practices may have influenced original appearance and corrosion processes during burial. In the case of Greek armour, it is known from Pausanias 1.15.4 [6] that the shields displayed in the Painted Stoa in Athens were cleaned and covered in pitch to preserve them [7]. The regular cleaning and protection of bronzes using oils, mentioned in ancient sources, could prevent corrosion during use [2] (p. 355) but it is unlikely that such maintenance-polishing would have preserved an ancient artificial patination. So far, in literature, a 'finishing patina' on ancient helmets is most often inferred from a combination of evidence deriving from ancient illustrations and literature, rather than its survival on metalwork itself. In practical terms, it is believed that it is challenging to discriminate between artificial patination and natural patinas using scientific methods alone [2] (pp. 352–353).

Corrosion of archaeological copper alloys during burial

Previous work showed that corrosion of archaeological bronzes during burial could result in the development of blue, green, brown and light or dark grey patinas that can preserve polishing marks [8–10]. Although polishing marks have been reported on tin-rich patinas that exhibit an even Type I corrosion [11], on low-tin α-bronzes [8] and on low-tin bronzes with an $\alpha+\delta$ cast microstructure, in literature polishing marks are predominantly reported on even patinas on high-tin archaeological bronzes [12–15] (p. 340). It is reported that the tin concentration in the tin-rich layer is related to the original tin concentration of the alloy [8–10]. The colour is reported to be a factor of the total amount of soil elements incorporated in the patina (mainly Si, P, Fe and Cl): bright grey patinas incorporate the least amount of soil elements and blue the most, with green patinas having amounts of soil intermediate between these two and dark green and dark grey have irregular soil element concentrations [8].

Robbiola et al [8] characterised the corrosion structure of archaeological bronzes based on the preservation of the marker of the original surface as: Type I for even or 'noble' corrosion surfaces that preserve original surface features and Type II which includes uneven or coarse or 'vile' patinas. There are several deviations from these proposed microstructural models; the tin-rich surface in Type I forms due to selective dissolution of copper during oxidation of the bronze [8] and consists of hydrated tin compounds, cupric compounds and a small amount of extraneous elements [9]. The two types are a result of different corrosion mechanisms. According to this model, corrosion growth in Type I structures proceeds inward, with oxygen and hydroxyl anions migrating inwards and copper cations migrating outwards controlling the corrosion process. Its formation is clearly related to a movement of oxygen anions inwards to the alloy, but further investigation is necessary to determine precisely if the process is under control of interfacial reactions or controlled by cationic reaction (Cu cations) or anionic oxygen migration. Such tin-rich corrosion is related to the original tin concentration of the bulk alloy and forms via inter-

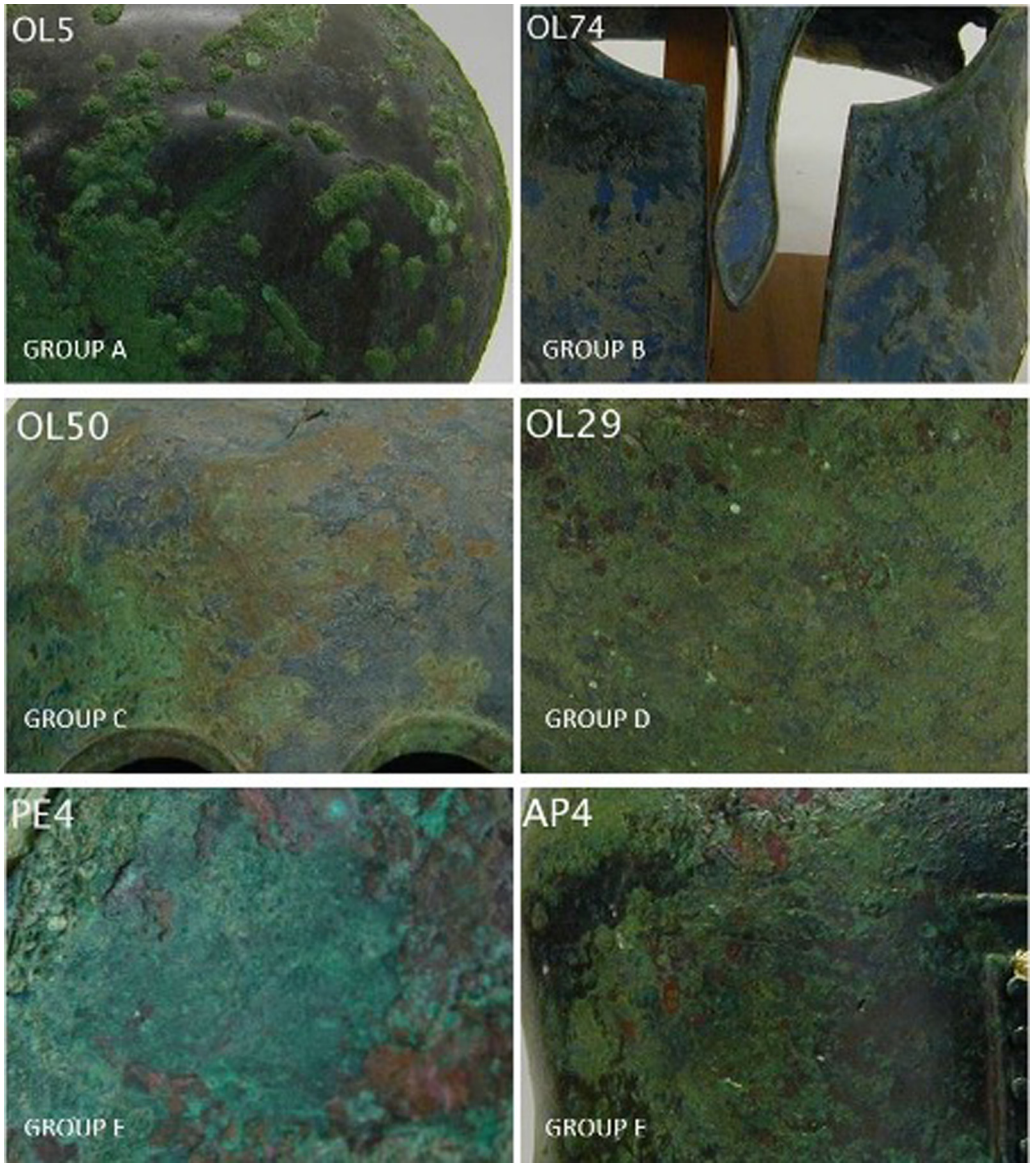

Fig. 1. Images of representative surface corrosion present on helmets, as grouped in Table 1.

nal oxidation phenomena characterised by the outward migration of copper cations (Cu^{+}, Cu^{++}) from the bronze and the inward migration of anions of soil elements (such as O, P, Si, Fe, Ca) [8]. In Type II structures, corrosion growth proceeds outwards, resulting in the loss of the marker of the original surface; copper cations migrate from the bronze surface to the aqueous environment, whilst anions migrate inwards and control the corrosion mechanism.

Generating more analytical data from low-tin archaeological bronzes will be useful to confirm and/or extend these existing classifications, and to further understanding of corrosion mechanisms and resulting formation of fine patinas. Because of the association of the word patina with what marks the original surface, this paper uses the word patina to refer to natural or artificial corrosion surfaces that preserve the marker of the original bronze surface onto which copper compounds are deposited as corrosion products from interaction with soil elements during burial. Naturally formed grey/silver or black patinas on low-tin bronzes may cause interpretation problems when assessed in the field as silvery or bright to dark grey surfaces on archaeological bronzes can look deceptively similar to corroded tin coatings [16] or silvering [17]. Understanding of what constitutes evidence of tinning on low-tin archaeological bronzes has been published [16,18] but more work is necessary to investigate the visual impact of a corroded metallic coating or corrosion resulting from a coating of a dissimilar metal on a low-tin bronze.

Materials and methods

This is part of a larger project involving the examination and documentation of 154 helmets from (a) excavations including the sanctuary at Olympia by the German Archaeological Institute, from Archaic period cemeteries held at the Archaeological Museum of Thessaloniki and helmets from the Archontiko cemetery at Pella; (b) helmets from collections belonging to the Ashmolean, the Pitt Rivers, the Fitzwilliam and the National Museum of Wales. Of those, 36 helmets were selected likely to be untreated and sampled from areas with undisturbed surfaces from cleaning to permit investigation of their fine grey, black or other corrosion surface and are presented in this study (Table 1) Permission to study and sample the helmets was formally issued by the Ministry of Culture-Greece (Related permissions: ΥΠΠΟ/ΣΥΝΤ/Φ44/3650/72468; 3297/63795; 2054/142699; and

Table 2
Characterisation of helmets/samples based on the abundance of azurite and/or malachite established by macroscopic qualitative observation.

Helmet/ Sample	Helmet side analysed	Surface appearance	Predominant deposit on helmet	Patina colour on helmet	Colours in Corrosion profiles
OL27.1	Outer	Group A	Malachite - pustules	Grey	B/B
OL31.1	Outer	Group A	Malachite - pustules	Black	B/B
OL5.1	Outer	Group A	Malachite - pustules	Black/grey	B/B
OL74.1	Outer	Group B	azurite / mal	Black	B/B
OL75.2	Inner	Group B	azurite / mal	Black	B/B
OL79.1	Inner	Group B	azurite / mal	Black	B/B
OL79.1	Outer	Group B	azurite / mal	Black	B/B
OL46.1	Outer	Group B	azurite / mal	Soiled	B/G
OL73.1	Outer	Group B	azurite / mal	Black/grey	B/G
OL75.2	Outer	Group B	azurite / mal	Black	B/G
OL71.1	Inner	Group C	azu / mal	Brown	B/B
OL49.1	Outer	Group C	azu - mal	Brown	B/G
OL57.2	Outer	Group C	azu - mal	Green	B/G
OL71.1	Outer	Group C	azu - mal	Brown	B/G
OL9.2	Outer	Group C	azu - mal	Green	B/G
OL9.2	Inner	Group C	azu / mal	Green	B/G
OL4.2	Outer	Group C	azu - mal	Green	B/G
OL50.1	Outer	Group C	azu - mal	Brown	B/G
OL78.1	Outer	Group C	azu - mal	Green	B/G
OL66.1	Outer	Group C	azu - mal	Green	B/R/G
OL58.1	Outer	Group D	mal / azu	Green	B/R/G
OL58.1	Inner	Group D	mal / azu	Green	B/R/G
OL78.1	Inner	Group D	mal / azu	Black	B/R/O/Y/G
PE1.1	Outer	Group D	mal / azu	Grey	B/R/O/Y/G
PR1.1	Outer	Group E	Malachite	Dark Green-Red	B/R/G
PR4.1	Outer	Group E	Malachite	Dark Green-Red	B/R/G
AP4.2	Outer	Group E	Malachite	Dark Green-Red	B/R/O/Y/G
AP5.1	Inner	Group E	Malachite	Dark Green-Red	B/R/O/Y/G
AP4.2	Inner	Group E	Malachite	Dark Green-Red	B/R/O/Y/G
AP5.1	Outer	Group E	Malachite	Dark Green-Red	B/R/O/Y/G
OL21.1	Outer	Group E	Malachite	Dark Green-Red	B/R/O/Y/G
OL21.1	Inner	Group E	Malachite	Green	B/R/O/Y/G
OL41.1	Outer	Group E	Malachite	Brown/Red	B/R/O/Y/G
OL44.1	Outer	Group E	Malachite	Brown/Red	B/R/O/Y/G
OL53.1	Inner	Group E	Malachite	Dark Green-Red	B/R/O/Y/G
OL53.1	Outer	Group E	Malachite	Dark Green-Red	B/R/O/Y/G

1860/35872). Sampling of metal cross-sections was performed by the author (PM) using metal cutters; a small fragment was removed from each helmet were possible within the conservation guidelines. Selected corrosion powders were removed for further investigation in several areas of the helmets.

The physical condition of the surface on the helmet samples was investigated using scanning electron microscopy (SEM) with backscattered electron imaging (BSE) employed in top-view before embedding the sample, and in cross-section of the embedded polished sample. Cross-sectional investigation of the surface of the samples was undertaken using SEM-BSE imaging, energy dispersive X-ray spectroscopy composition analyses (SEM-EDX), SEM-EDX mapping and bright-field polarised microscopy (BFOM). These methods were also used to investigate the manufacture and the composition of the helmets, results of which are to be reported in detail elsewhere. Metallurgical evaluation was supported by macroscopic observations, x-radiography, and neutron diffraction texture analysis of selected helmets [19]. CuKα X-ray diffraction (XRD) at the National Museum of Wales and synchrotron radiation X-ray diffraction (SR-XRD) at Daresbury Laboratory (SRS, Synchrotron Radiation Source UK) were used selectively [20] to characterise crystalline corrosion compounds on archaeological samples.

The surface condition of all samples was evaluated and documented prior to their analysis, using a Nikon SMZ1000^{TM} stereomicroscope fitted with a Nikon CoolPix 4500^{TM} camera. Samples were mount in Struers Epofix^{TM} epoxy resin, and their sections were ground and polished using the Struers Labopol-5^{TM} with progressively finer grit of silicon carbide papers (180- 4000) and Metadi^{TM} diamond polishing pastes (3–1/4 µm). Non-aqueous media and white spirit were used for polishing all archaeological samples to prevent dissolution of water-soluble species such as chloride from the corrosion layers. Polished blocks were kept in desiccated storage prior to analysis. Samples were carbon coated for both top-view before embedding in resin and cross-sectional SEM observation using the Emitech K450^{TM} Carbon Coater with carbon fibre strands.

Compositional analysis employed a CamScan 2040 SEM (20 kV with 120 × 96 μm spot area) with an Oxford Link Pentafet 5518 Dispersive X-ray spectrometer and the Isis 300 software, housed at the Conservation Section Laboratories at Cardiff University. The spectrometer's super thin atmosphere window (ATW2) permits X-ray detection of light elements ($Z>4$). Calibration involved pure elements, mineral and bronze standards (No. 4629, from Micro-Analysis Consultants Ltd). Oxygen calibration used wollastonite ($CaSiO_3$) and showed 1.8% mean relative error of accuracy and 1% relative precision on the oxygen wt% measurements. All reported analysis is the average of at least three area analysis of the same feature. Accuracy and precision were reduced when analysing corroded surfaces as micro-roughness is inevitably encountered after polishing due to hardness differences and some loss of material on the corrosion layers.

X-ray diffraction (XRD) was undertaken using an XPERT-PRO PANalytical X-Ray diffractometer at the National Museum of Wales, Cardiff. Selected flat samples were analysed *in situ* on a fixed stage with divergent beam footprint of 100 or 200 mm^2 for 20–60 min acquisition time depending on the sample. Data was analysed with the X'Pert HighScore V2.1.2 software using the PDF-02 database, with the 2005 Release ICDD library. A small number of samples was analysed using Synchrotron-XRD at Daresbury SRS Facility UK

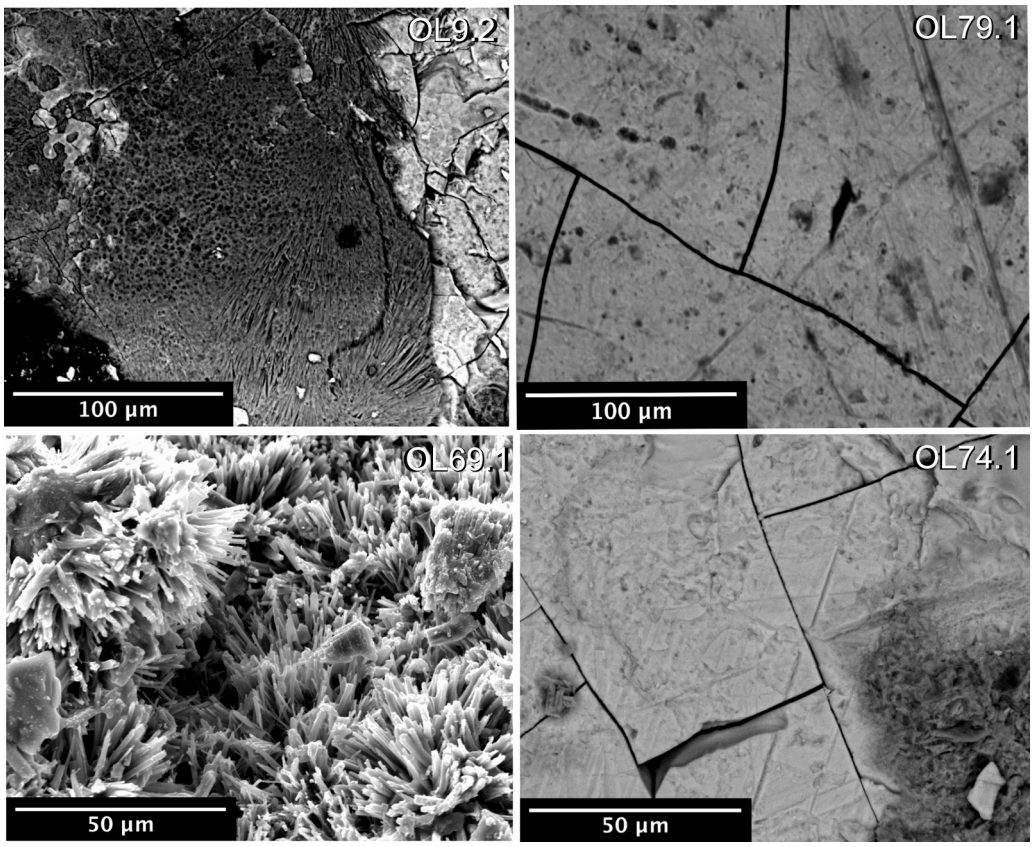

Fig. 2. Selected SEM-BSE images of the surface of helmet samples showing polishing marks preserved in the smooth patina marking the original surface layer (MOS) [OL79.1, OL74.1]. OL9.2 shows top-view SEM-BSE and characteristic morphology of corrosion deposits - flat layer of fibrous corrosion situated between a flat compact corrosion layer and porous MOS that resembles the fibrous nature of the deposit. OL69.1: SEI detail of 'sea urchin' like corrosion deposit. The scale is 50 μm at X500 and 20 μm at x1000 magnification.

using reflection geometry at beamline 10.1 and in transmission geometry at beamline 14.1 [20].

Results

Macroscopic surface characterisation of the helmets

The fineness and colour of the surface of the helmets and samples was characterised using simple qualitative criteria. Although visual observation and colour assessment is subjective, its use here makes the results more relevant to common practice in the field. The helmets were grouped based on the prevalent colour of their corrosion deposits and the colour of the exposed underlying fine corrosion layer (patina) if present (Fig. 1; Table 2). Helmets in Group A exhibit localised voluminous malachite pustules (confirmed with XRD) with areas of smooth grey or black patina. Helmets OL5 and OL31 from this group have azurite deposits (confirmed with XRD) on their inner sides. The characteristic malachite morphology is used to group these helmets. Group B comprises helmets with predominantly azurite deposits and a fine black or grey patina, which is largely free of deposits on several of the helmets. Group C is formed from helmets that are largely covered by azurite and malachite deposits with a brown or green patina. In Group D helmets, malachite is more abundant relative to azurite and the patina appears dark-green or brown with areas of a red surface exposed. Group E helmets have areas of exposed dark or red patinas covered by malachite (confirmed with XRD), which is in mostly voluminous (e.g. PE4, AP4, AP5, PR1).

This basic, preliminary, macroscopic assessment shows that a finer patina is more frequently observed on helmets where blue deposits predominate. The exposed patina is finer in these groups and, in several cases, the patina appears black or grey (Group B). When the deposits of malachite (confirmed with XRD) are more prevalent on a helmet, the underlying patina appears brown to dark red in colour, indicating that the underlying layer contains cuprite (Group E) (Table 2). These observations form the hypothesis that fine black or grey and red/brown patinas are related to different burial corrosion processes favouring the formation of azurite or malachite deposits. In general, red patinas are encountered with malachite deposits and black or grey patinas are predominantly found in the presence of azurite.

X-Ray diffraction of crystalline surface corrosion products

Fifteen samples of representative crystalline corrosion deposits in the form of powders or *in situ* directly on the sample surface) were analysed using CuKα XRD or SR-XRD to characterise them. Analysis confirmed that the blue deposit found on several samples is azurite and the dark green/green deposit is malachite, confirming earlier visual identification of these products. Analysis from the surface of selected samples confirmed the presence of cuprite (dark red / brown patine).

Of particular interest are helmets OL79, PE1 and OL74 (Fig. 1, supplementary material), because of their fine smooth dark grey/black, grey and dark green patina, respectively. SR-X ray diffraction analysis in reflection geometry on the surface of fragments from these helmets shows that the patinas of OL79 and PE1 are composed predominantly of azurite and for OL74 both malachite and azurite. Silica is present on OL74 and OL79 in a small amount and cuprite is detected on PE1. Cassiterite or other crys-

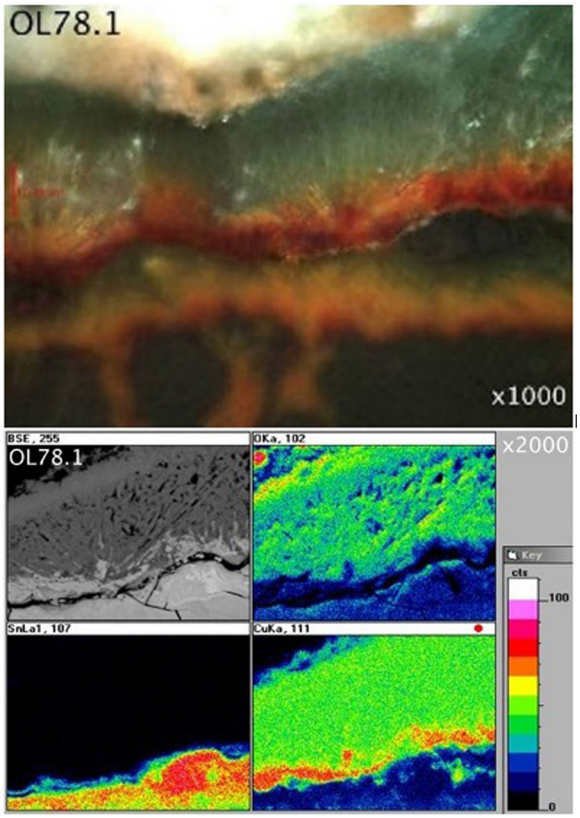

Fig. 3. BFOM, SEM-BSE image and EDX maps of OKα, SnLα and CuKα, showing 'sea-urchin' shaped spiky malachite crystals elongating from a spiky cuprite layer. The key notes x-ray counts for CuKα. Sample OL78.1 inner helmet side.

talline tin-oxide was not detected using this methodology (Fig. 1, supplementary material).

SEM-BSE imaging of the surface (top-view) of the samples

SEM-BSE examination of the surface of un-mounted samples recorded the smooth corroded surface (patina) preserved on the majority of the samples. A smooth but often cracked patina preserves polishing marks and it forms the marker of the original surface, which is visible when it is free of corrosion deposits (Fig. 2). In one case (OL74.1), polishing marks that were preserved on the patina were imprinted on the underside surface of a flaked off layer of azurite (confirmed by SR-XRD). This suggests that these abrasions are evidence of polishing in antiquity, rather than a post excavation 'cleaning' process. BSE observation at high magnifications determined that 12 helmets retained evidence of polishing marks on the marker layer for the original surface (MOS). For 11 of the helmets overlying corrosion deposits obstructed close observation of their surface. Polishing marks are detected mainly on the surface of samples from helmets in Group A and B either because they are relatively free of corrosion deposits or deposits only cover them locally.

Fig. 2 shows additional morphological examples of corrosion deposits covering the surface. OL9.2 has a layered corrosion deposit, where a flat and compact outer layer overlays a fibrous corrosion deposit. Thicker corrosion deposits composed of several layers predominate on samples from Group E and a smooth marker of the original surface is not visible, being either obscured by this corrosion deposit or absent beneath it (OL69.1). The exterior layers of these deposits often have a spiky 'sea-urchin' like appearance at high magnification (Fig. 3). Elemental analysis of cross sections revealed copper and oxygen concentrations to be high in these areas and combined with its green colouration it was thought to be malachite with a base of cuprite (OL78.1, Fig. 3).

SEM-BSE and BFOM imaging of the cross-sectioned samples

The corrosion profile of the zone below the marker of original surface (MOS) was characterised based on the number of corrosion zones within the corrosion profile and the presence or absence of an inner cuprite zone at the patina/bronze interface. With the exception of two samples that have a single fine corrosion layer (Corrosion Profile 1, Fig. 4), cross-sections exhibit two corrosion zones below the marker of the original surface. Several of the samples with two corrosion zones exhibit a characteristic cuprite red and/or orange/yellow inner corrosion zone visible in Bright Field Polarised Microscopy, the lower limit of which interfaces with the bronze (Corrosion Profile 4, Fig. 4). The colour of the outer corrosion zone, the upper limit of which is the MOS, varies from light to dark green in these samples. Several samples that do not have an inner red/yellow zone (Corrosion Profile 2, Fig. 4) have a fibrous microstructure or an unusual chemical distribution of major elements seen in SEM-EDX maps. A small number of samples exhibit different characteristics when comparing the inner and outer side of the helmet.

The corrosion profiles in the samples are characterised by the following description:

- Corrosion Profile 1: includes samples that exhibit a single, relatively uniform corrosion zone between the marker of original surface (MOS) and the bronze metal.
- Corrosion Profile 2: includes samples that exhibit two corrosion zones (outer and inner) and are free of cuprite or orange/yellow compounds at the inner corrosion zone. This group includes samples with characteristic fibrous microstructure mainly present at the inner zone. The outer part of the patina is black, blue or light green/blue in colour and it is not covered extensively by deposits.
- Corrosion Profile 3: includes samples that do not exhibit a fibrous microstructure, similar in cases to Piccardo's 'tentacle-like' corrosion features [21], although some samples have intergranular corrosion filaments in the bronze and are covered extensively by corrosion deposits; they can have localised patches of cuprite-red or a thin inner zone of red, orange/yellow inner compounds with no evidence of preserved slip lines in this zone.
- Corrosion Profile 4: includes samples with a cuprite layer present at the inner corrosion zone. This group includes samples with a thick distinctive cuprite or orange/yellow inner zone, which preserves extensive evidence of preserved slip lines in this zone.

Samples in Corrosion Profile 4 exhibit fine straight lines that are either parallel or cross each other in batches, with each batch seeming to have a different orientation (Fig. 5). These lines resemble slip lines observed in work-hardened α-bronze grains seen in the metallic bronze. This indicates cuprite can preserve the metallographic structure of the bronze in the form of pseudomorphs, which must occur via an *in-situ* corrosion diffusion mechanism. Characteristically, this evidence of strain stops at the inner/outer corrosion zone interface where a green corrosion zone starts as an outer layer. A schematic of profiles 3 and 4 is shown in Fig. 2-supplementary material.

SEM-EDX composition of the core metal

SEM-EDX composition analysis of the core metal of the samples showed that they are made of low tin with concentrations between c. 5 and 14 wt% (wt%) Sn ($\pm$ 0.1 to 0.4 Standard Deviation).

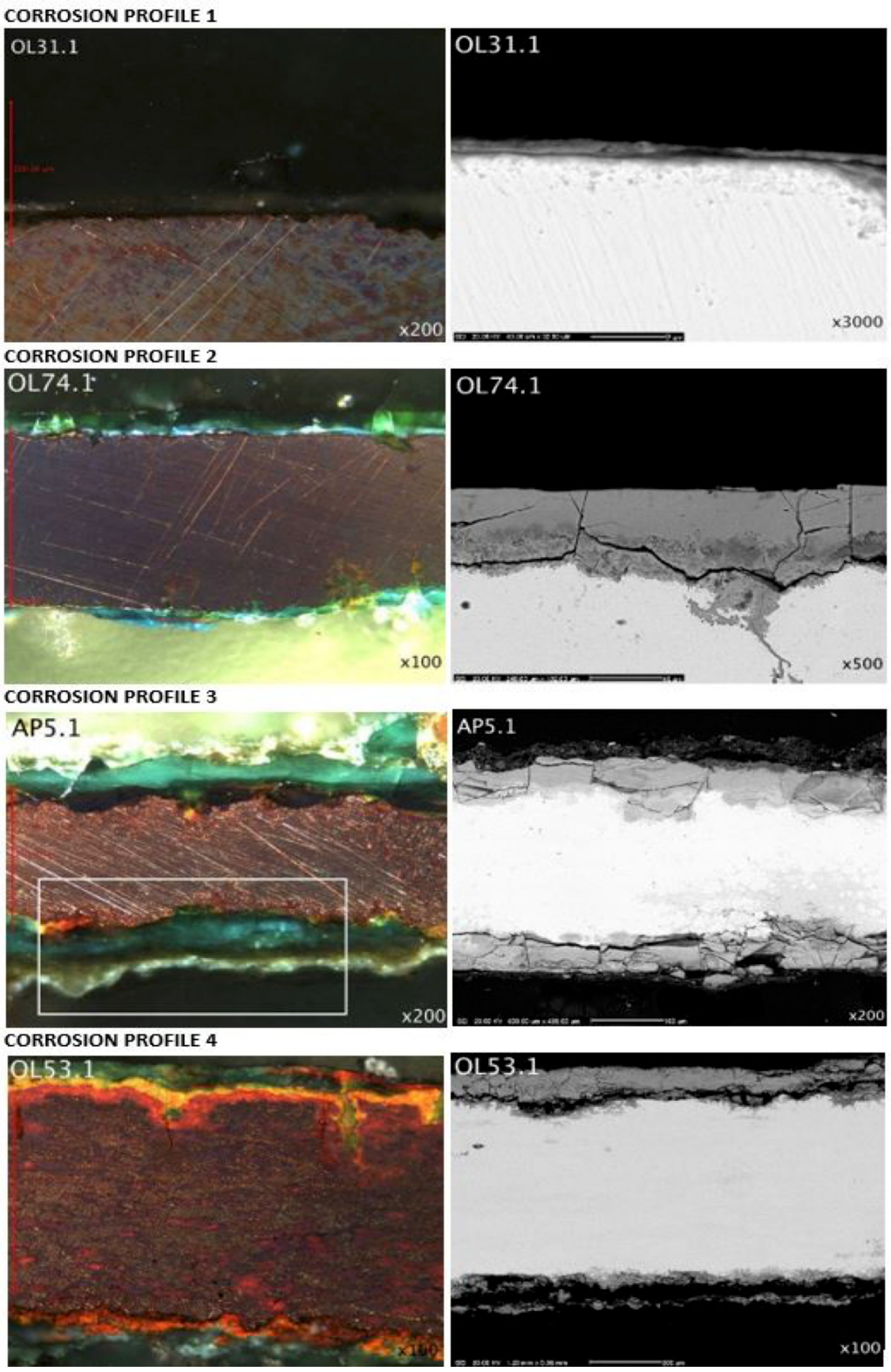

Fig. 4. Images of polished cross-sectioned samples showing characteristic corrosion profiles, with or without corrosion deposits on the corroded surface. Left column: BFOM Images. Right column: SEM-BSE Images of the same sample.

The samples are homogenised α-bronzes produced by hammering; the presence of twinned grains and the reduced grain-size is clear evidence that the helmets were exposed to cycles of cold working and annealing. Reduction in grain size and thickness by cold working increases the tensile strength of a given solid solution in a reproducible quantitative manner [22] (p. 66). Extensive hammering can also result in banding of alloying elements, which in turn could affect corrosion of the core, and likely the surface corrosion and appearance of an object. Intensive hammering may explain the preferential banded tin depletion and corrosion observed in some

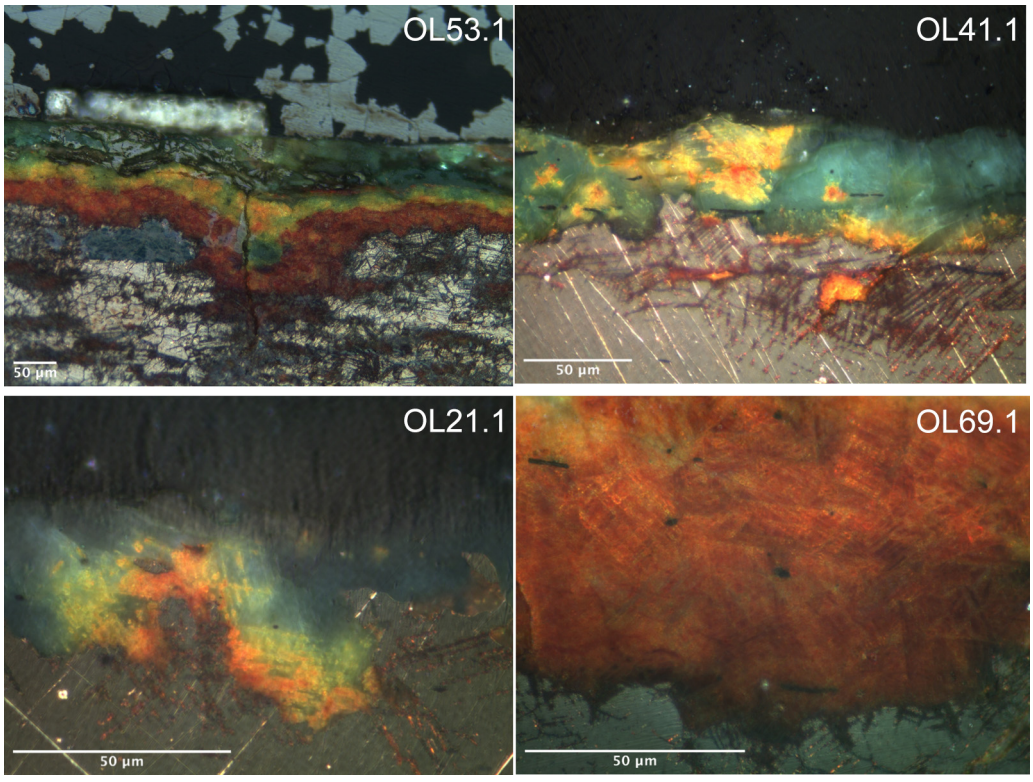

Fig. 5. BFOM images showing cuprite and/or orange yellow compounds forming an inner corrosion zone. OL69.1: detail showing fine straight line pseudomorphs of slip lines. OL53.1: slightly etched polished section showing slip lines in the strained work-hardened α-bronze grains continuing into the cuprite zone. OL21.1 and OL41.1: detail showing cuprite slip line pseudomorphs changing into orange/yellow colour as they elongate into the green/blue outer corrosion zone where they are no longer visible in BFOM images.

samples. This agrees with a previously published sample from a 10 wt% Sn Greek bronze shield (5th c. BC), which exhibits banding interpreted to be due to intensive hammering and which in turn resulted in the fine white/grey cassiterite layer present on the surface [23]. XRD did not confirm the presence of cassiterite on any of the samples, here.

SEM-EDX composition analysis of corrosion layers in cross-sections

Table 3 records SEM-EDX wt% composition analysis averaged from at least 3 area/spot analysis on each feature of interest in the cross section of each helmet sample. Data shows that the composition of the outer part in the patina is richer in Sn compared to the inner zone. Loss of Cu is related to the uptake of O; Total Soil Elements (TSE) tend to appear elevated with elevated Sn concentration at the outer surface. The number of elements that are incorporated from the soil such as Si, P, Fe, Al, Cr are expected to be proportional to the decuprification and the dissolution of copper is evident by the uptake of the amount of oxygen, where low Cu coincides with high O and vice versa (Fig. 3, supplementary material). The Sn-enrichment observed in the outer corrosion zone due to the dissolution of copper is related to the original Sn concentration of the low-Sn bronze alloy (Fig. 3, supplementary material). The colour of the patina is influenced by the amount of soil elements present, as the black/grey patinas have the highest amounts of silica (Fig. 4, supplementary material).

Plotting the Cu, Sn, O Atomic% (at%) normalised concentration on a ternary diagram (Fig. 6) shows that data from inner cuprite zones from samples grouped in CP3 and CP4 are on a distinct area of the ternary diagram. Data from copper carbonate deposits are also shown. The positions of tin oxides are plotted for reference. Samples that cluster at the area with higher Sn concentrations are visible as fine black, black/grey patinas.

Discussion

Results show that samples have:

(a) fine black or grey smooth patinas often with a fibrous microstructure associated with azurite;

(b) smooth patinas with an inner cuprite/cuprite rich zone, which appear red/brown macroscopically often associated with the predominant presence of malachite although azurite can be present on the helmet;

(c) patinas with a broadly defined but uneven marker of the original surface that is extensively covered by malachite.

Malachite and azurite develop under different burial conditions, depending on the amount of dissolved CO_2, pH, temperature, dissolved ions amongst other factors [24]. Although the burial conditions of the helmets are unknown, data indicate that the corrosion profile of patinas is linked to the abundance of azurite or malachite deposited on their surface. Helmets covered predominantly by azurite exhibit black or silver/grey patinas, while those covered by malachite have a red/green patina.

Smooth black/grey or red/brown patinas on helmet samples are rich in oxygen and exhibit higher tin-concentration in the outer zone compared to their lower-tin inner zones. Samples with an uneven MOS have a lower tin-concentration in their outer corrosion zone, and when plotted on the Cu-Sn-O Atomic% ternary diagram their composition is located towards that of copper carbonates in the plot (Fig. 6). The inner corrosion zone at the interface with the remaining metallic bronze can contain lower tin-concentration or no detectable tin at the areas of cuprite-red. Cuprite was detected on samples of this group (e.g. OL53, OL69). The orange/yellow fea-

Table 3
SEM-EDX weight% composition normalised on the analysed elements; data is of corrosion features in the corrosion profiles.

Helmet Sample	Analyses code	Helmet side analysed	Corrosion zone	O	Al	Si	P	S	Cl	Ca	Cr	Fe	Cu	Zn	Sn
AP4.2	AP4.2_L2O	Inner	Outer	21.5	0.0	0.6	3.3	0.1	0.1	1.7	0.0	0.4	52.4	0.0	20.1
	AP4.2_LI	Outer	Inner	17.3	0.0	0.3	0.0	0.5	1.1	0.1	0.0	0.1	68.5	0.0	12.2
	AP4.2_LO	Outer	Outer	34.0	0.0	0.7	0.2	0.2	0.1	0.4	0.0	0.2	48.7	0.0	15.5
AP5.1	AP5.1_L2I	Inner	Inner	16.8	0.0	0.3	0.2	0.7	0.9	0.1	0.0	0.2	68.3	0.0	12.4
	AP5.1_L2O	Inner	Outer	36.2	0.0	1.1	1.6	0.3	0.2	0.7	0.0	0.2	43.2	0.1	16.5
	AP5.1_LI	Outer	Inner	34.7	0.0	0.6	5.1	0.3	1.1	1.3	0.0	0.3	40.4	0.1	16.1
	AP5.1_LO	Outer	Outer	30.7	0.0	0.6	5.9	0.2	1.4	2.1	0.0	0.3	32.6	0.0	26.0
OL13.1	OL13.1_LO	Outer	Outermost	26.4	0.1	2.2	0.6	0.0	0.0	0.7	0.1	1.2	25.6	0.1	43.0
OL21.1	OL21.1_L2O	Inner	Outer	32.0	0.1	4.2	0.1	0.3	0.0	0.7	0.0	0.4	16.4	0.1	45.5
	OL21.1_LI	Outer	Inner	36.1	0.0	3.6	0.2	0.2	0.3	0.5	0.0	0.4	23.8	0.0	34.8
	OL21.1_LO	Outer	Outer	31.6	0.1	4.0	0.1	0.3	0.1	0.7	0.0	0.4	15.0	0.0	47.5
OL27.1	OL27.1_L2O	Outer	Outermost	30.1	0.1	2.8	1.2	0.1	0.2	1.2	0.0	0.6	20.4	0.0	43.3
	OL27.1_LO	Outer	Outer	30.8	0.0	1.7	1.4	0.0	0.0	1.0	0.1	0.6	22.5	0.1	41.6
OL31.1	OL31.1_LO	Outer	Outer	33.2	0.1	1.8	4.6	0.1	0.1	3.0	0.1	4.5	16.0	0.1	36.4
OL4.2	OL4.2_LD	Outer	Deposit	33.7	0.1	0.1	0.2	0.0	0.1	0.1	0.0	0.1	65.5	0.0	0.2
	OL4.2_LO	Outer	Outer	27.4	0.1	1.5	0.4	0.1	0.1	0.4	0.0	0.9	30.6	0.1	38.5
OL41.1	OL41.1_LI	Outer	Inner	31.4	0.0	1.7	0.6	0.1	0.1	0.3	0.0	0.6	36.6	0.1	28.4
	OL41.1_LO	Outer	Outer	34.6	0.2	2.5	0.5	0.2	0.1	0.8	0.1	1.8	18.8	0.1	40.5
OL44.1	OL44.1_LI	Outer	Inner	18.1	0.0	0.6	0.0	0.1	0.1	0.2	0.1	0.3	66.2	0.0	14.3
	OL44.1_LO	Outer	Outer	32.7	0.1	3.2	0.3	0.1	0.0	1.1	0.4	0.7	14.9	0.0	46.6
OL46.1	OL46.1_LD_1	Inner	Deposit	31.7	0.3	0.8	0.2	0.0	0.0	0.6	0.0	0.3	66.1	0.1	0.0
	OL46.1_LI	Outer	Inner	39.0	0.1	3.2	1.6	0.2	0.1	0.9	0.3	0.6	22.5	0.0	31.6
	OL46.1_LO	Outer	Outer	33.9	0.1	3.2	1.1	0.7	0.1	0.8	0.5	0.9	15.0	0.3	43.5
OL49.1	OL49.1_LO	Outer	Outer	32.4	0.0	3.8	0.1	0.1	0.1	0.7	1.5	0.8	11.8	0.0	49.1
OL5.1	OL5.1_LI	Outer	Inner	32.9	0.1	2.7	0.2	0.1	0.1	0.7	0.1	0.5	20.8	1.9	40.0
	OL5.1_LO	Outer	Outer	28.0	0.2	4.0	0.3	0.2	0.1	1.1	0.3	0.6	15.8	3.7	45.9
OL50.1	OL50.1_LD	Outer	Deposit	37.7	0.0	0.1	0.0	0.0	0.0	0.1	0.0	0.5	61.2	0.1	0.2
	OL50.1_LI	Outer	Inner	21.9	0.0	2.5	0.2	0.5	0.1	1.1	0.3	0.8	39.5	0.0	33.1
	OL50.1_LO	Outer	Outer	33.6	0.0	2.5	0.2	0.2	0.1	0.4	0.0	1.6	34.3	0.0	27.0
OL53.1	OL53.1_L2O	Inner	Outer	36.5	0.0	3.9	1.2	0.0	0.0	1.2	0.5	1.1	19.6	0.0	36.0
	OL53.1_LI	Outer	Inner	30.5	0.0	1.5	0.7	0.1	0.1	0.6	0.0	2.1	29.2	0.1	35.2
	OL53.1_LO	Outer	Outer	31.0	0.0	3.5	1.2	0.2	0.1	1.3	0.7	1.2	20.4	0.0	40.4
OL57.2	OL57.2_LI	Outer	Inner	30.0	0.0	2.7	1.5	0.0	0.3	1.2	0.8	1.2	23.4	0.1	38.8
	OL57.2_LO	Outer	Outer	32.5	0.2	4.0	1.9	0.2	0.1	1.6	0.6	2.1	14.5	0.1	42.3
OL58.1	OL58.1_L2O	Inner	Outer	34.2	0.0	0.8	1.0	0.1	0.0	0.5	0.0	0.2	36.2	0.3	26.6
	OL58.1_L2Ob	Outer	Outermost	34.1	0.0	0.1	0.8	0.0	0.1	0.2	0.3	0.9	39.7	0.2	23.5
	OL58.1_LO	Outer	Outer	33.9	0.0	0.4	0.8	0.8	0.0	0.3	0.0	0.2	40.1	0.1	23.4
OL66.1	OL66.1_LO	Outer	Outer	31.1	0.0	1.4	1.3	0.0	0.0	0.8	0.0	0.8	40.1	0.0	24.5
OL70.1	OL70.1_LD	Outer	Deposit	34.5	0.1	0.4	0.1	0.0	0.0	0.3	0.0	0.1	62.9	0.0	1.5
OL71.1	OL71.1_L2O	Inner	Outer	19.6	0.2	2.1	0.0	0.1	0.0	1.0	0.8	0.5	33.3	0.1	42.3
	OL71.1_LI	Outer	Inner	36.1	0.1	3.4	0.0	0.1	0.1	0.8	0.8	0.1	19.7	0.0	38.8
	OL71.1_LO	Outer	Outer	34.7	0.2	4.5	0.1	0.2	0.1	1.2	1.7	0.1	10.3	0.0	47.0
OL73.1	OL73.1_LO	Outer	Outer	30.2	0.1	3.5	0.0	0.1	0.0	0.6	0.8	0.6	17.0	0.0	47.0
OL74.1	OL74.1_cpd	Inner	Deposit	35.3	0.3	0.9	0.1	0.0	0.1	0.3	0.0	0.2	62.5	0.1	0.1
	OL74.1_L-band	Inner	Outermost	25.6	0.1	3.7	0.3	0.1	0.1	1.0	0.3	0.4	21.4	0.0	47.2
	OL74.1_LO	Outer	Outer	34.7	0.1	3.9	0.1	0.1	0.1	0.9	0.5	0.5	14.9	0.0	44.3
OL75.2	OL75.2_L2O	Inner	Outer	27.2	0.1	3.2	0.2	0.0	0.1	1.0	0.1	2.1	16.0	0.1	49.9
	OL75.2_LO	Outer	Outer	36.9	0.1	4.0	0.1	0.1	0.1	1.1	1.5	0.3	11.2	0.0	44.6
OL78.1	OL78.1_L2O	Outer	Outer	33.8	0.3	2.5	0.9	0.1	0.1	1.1	1.3	1.5	13.6	0.1	44.6
	OL78.1_LI	Inner	Inner	21.8	0.1	0.5	0.0	0.0	0.3	0.2	0.0	0.2	53.1	0.0	23.7
	OL78.1_LO	Inner	Outer	32.5	0.1	1.1	0.3	0.1	0.2	0.4	0.0	1.6	30.9	0.0	32.8
OL79.1	OL79.1_L2O	Inner	Outer	33.3	0.1	2.7	0.5	0.1	0.0	1.0	0.3	1.7	20.6	0.1	39.6
	OL79.1_LI	Outer	Inner	32.8	0.1	3.1	0.7	0.0	0.0	1.3	0.7	1.8	16.5	0.0	42.9
	OL79.1_LO	Outer	Outer	31.0	0.1	3.8	0.9	0.0	0.0	1.9	0.7	2.5	13.2	0.0	45.7
OL9.2	OL9.2_L2O	Inner	Outer	34.4	0.3	4.7	0.1	0.2	0.0	1.2	1.1	1.0	8.8	0.1	48.1
	OL9.2_LO	Outer	Outer	32.7	0.3	4.3	0.1	0.3	0.1	1.3	0.8	1.0	9.7	0.0	49.4
PE1.1	PE1.1_LI	Outer	Inner	20.1	0.0	0.8	0.4	0.1	0.2	0.1	0.0	0.1	55.8	0.0	22.3
	PE1.1_LO	Outer	Outer	29.4	0.1	0.7	0.1	0.2	0.0	0.3	0.0	0.2	24.3	0.1	44.7
PE1.2	PE1.2_LI	Outer	Inner	24.3	0.0	1.8	0.4	0.1	0.1	0.3	0.0	0.2	44.6	0.1	28.2
PR1.1	PR1.1_LO	Outer	Outer	31.5	0.0	1.2	0.9	0.6	2.0	1.1	0.0	0.2	34.0	0.3	28.2
PR4.1	PR4.1_LO	Outer	Outer	25.4	0.1	1.1	0.6	0.2	0.4	0.6	0.0	2.8	37.6	0.0	31.4

tures contain tin, have lower oxygen and increased copper concentrations relative to the bulk of the patina (Fig. 6). Published analysis reports that orange/yellow corrosion sites are a mixture of cuprite and hydrated SnO_2 oxides [9].

During oxidation, once the first corrosion layers form at an atomic scale, oxide film growth occurs via transport of metal cations or oxide anions (or both) through the oxide layer until a steady state is reached [25]. The ionic and electronic properties of the corrosion film are important because [26] formation of noble patinas is related to movement of oxygen anions through the corrosion zone [27]. The point defect model for steady state growth of passive corrosion films explains that migration of ions during aqueous corrosion occurs via the migration of anion and cation vacancies in the growing oxide crystal lattice in contact with a solution [28], assuming that the oxide film is crystalline but contains crystal point defects. Where the concentration of point defects is large enough, the film may be regarded as amorphous [29]. More analysis is necessary to confirm this hypothesis . In the case of inward corrosion growth, corrosion is controlled by the availability of anion vacancies in the corrosion film [30].

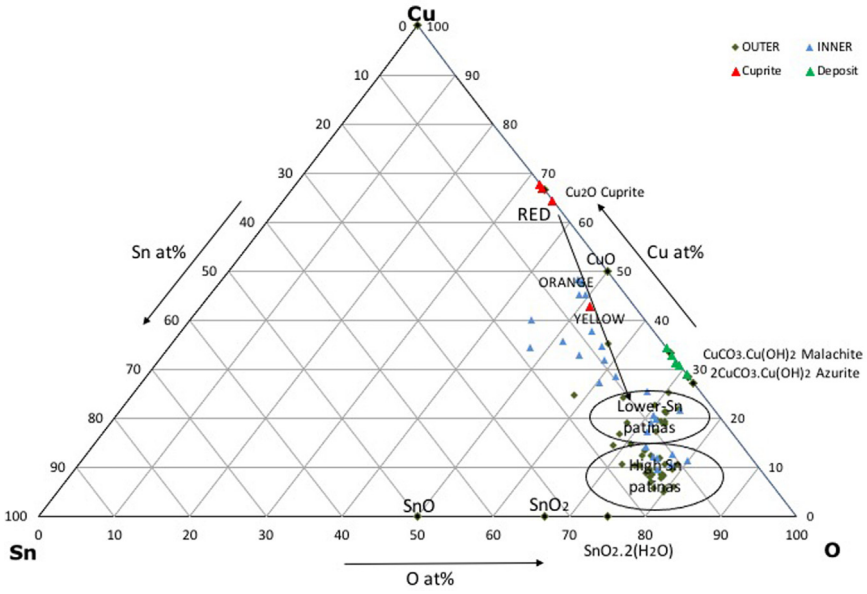

Fig. 6. Cu-Sn-O at% composition ternary plot showing the relationships between Cu, Sn, and O of the outer and inner corrosion zones in the corrosion profiles for samples in all groups. Data is averaged of 3 analysis spots per sample and per area analysed. Data from cuprite and copper carbonate deposits are also shown. The positions of tin and copper oxides and copper carbonates are plotted for reference.

Fine grey/black patinas associated with azurite

In the case of fine black or grey smooth patinas (described in (a) above), it is likely that oxidation of Sn to Sn(II) oxide takes place early in the corrosion process at a lower potential than the oxidation of Cu [31,32] and is followed by the formation of a Cu(I) oxide rich phase and Cu(II) species; then Sn-enrichment occurs in the outer corrosion layer because of the dissolution and relative loss of copper compared to tin, which remains in the patina due to the low solubility and high stability of tin species [27,32]. Published analysis shows that the outer part of the patina is composed of a mixture of Cu^{2+} compounds and sparingly crystalline $SnO_2.2H_2O$ [9]. Crystalline Sn-compounds were not detected on the samples during this work. It is reported that the low solubility of $SnO_2.2H_2O$ against a wide range of pH conditions, results in the formation of a physical and chemical barrier against the corrosive environment encouraging negligible rates of corrosion [33,34].

According to the equilibrium Eh-pH diagram of the Cu-CO_2-H_2O system, azurite is stable at acidic to neutral pH and to higher concentrations of dissolved carbonate [24]. During corrosion, the formation of corrosion products releases hydrogen ions into the solution decreasing local pH [35]. Assuming that the system behaves locally as a closed system, the form of carbonate in water depends on pH [36] (p. 37). Dissolved carbonate must exist chiefly as HCO_3^-n intermediate pH range and as $CO_3^{2-}n$ basic solutions [35]. Low pH favours the presence of H_2CO_3, which continuously provides hydrogen ions in the water. Increased availability of hydrogen ions, due to the increased dissolved carbonate in acidic conditions enhances the uptake of oxygen and metal dissolution. This is because the system provides H^+ to assist the cathodic half reaction [37], which occurs when pH is sufficiently low. In turn, this induces a reduction in the amount of dissolved oxygen due to oxygen consumption by copper corrosion [36] .

Fine red/brown patinas associated with malachite deposits

It is characteristic to this group (c) that in the presence of cuprite at the inner zone slip lines are preserved as pseudomorphic metallurgical evidence of the bronze microstructure due to extensive cold working. On the contrary, samples in (b) which includes samples with smooth patinas and with an inner cuprite/cuprite rich zone, they do not show evidence of slip lines and are covered localy by either malachite or azurite. Recent works have shown that the copper crystal orientation may impact the nature of the cuprite layer that is formed, producing epitactic relationships to the underlying copper that maintains defined crystallographic orientations [38]. It may be that the copper-crystal orientation produced by manufacturing influences the formation of a stable epitactic cuprite inner layer by favouring *in situ* oxidation of copper. It is thus likely that the extensive hammering of the helmets is influencing the development of smooth patinas.

Inner zones where cuprite is present do not contain any detectable Sn, unlike the orange/yellow compounds which contain Sn, Cu and O evidenced by the SEM-EDX data. It may be that growth of the cuprite zone was slow and the Eh/pH local conditions favoured dissolution of Sn and transport of Sn ions from the layer. Migration of Sn and Cu species from the inner zone would depend also on kinetic factors and the conductive properties of cuprite, which is pH dependent and at pH about 4 it shows an amphoteric acceptor/donor relationship [39].

Soil elements

The majority of the samples which exhibit a fine black/grey patina is associated with the presence of azurite deposit and they have high contents of Sn/Cu, O as well as soil elements (TSE) especially Si and Cr (Tables 2 and 3). Chromate ions act as oxidising agents or a source of insoluble films by formation of Cr_2O_3 [40]. A crystalline chromium-based compound was not identified on the helmet samples using diffraction methods, but analyses showed that measurable Cr-concentrations appear in the corrosion profiles at advanced Cu-dissolution levels. Early literature reports that potassium chromate was used as a corrosion inhibitor to prevent the corrosion of iron in an aqueous medium during washing processes requiring long periods of soaking [41] . However, it is unlikely that the chromate in this case is a residue of a past conservation treatment because the samples were selected from undisturbed areas of helmets. Literature shows that chromates in the aqueous environment accelerate the cathodic reaction of several metals in acidic conditions or act as a corrosion inhibitor if

the potential is raised to the passive regime [40]. Acceleration of the cathodic half reaction at an early point could have led to the faster dissolution of Cu from the bronze helmet samples leaving in place a Sn-rich patina. This could have slowed down the growth or the presence of an inner cuprite zone.

Chromium is rarely reported on archaeological patinas. Its presence has been associated with black patinas on Chinese bronzes but its existence due to intentional surface treatment is debated. In addition, the actual role of soil elements and their threshold concentrations in the development of coloured smooth patinas is not clear, especially with regards to the silver/grey and black patinas. For instance, it was suggested that the presence of 2wt% chromium found in the patina of a c. 12 wt% Sn (with c. 2 wt% Pb) Chinese bronze spearhead was responsible for its smooth black patina and corrosion resistant properties [42]. X-ray Diffraction confirmed the presence of CrO_2 and SnO on that object. This was attributed to intentional patination, although other small finds with similar patina found in the same burial context did not contain such a significant amount of chromium (0.2 wt%) [42], leading Meeks [43] to dispute the hypothesis of intentional patination of these Chinese bronzes, attributing the presence of the black surface to corrosion phenomena. More recent work offers further evidence for the non-intentional presence of chromium on Chinese bronzes [44].

Chromium exists in the environment in the trivalent Cr_{III} or hexavalent Cr_{VI} form and its natural source are chromite minerals ($FeCr_2O_4$). Relatively high levels of Cr often occur naturally in Greek waters due to their passage through chromite deposits [45] that occur widely in Greece. Occurrences include at Domokos, Vourino at Volos [46]:315, Rodiani [47]:98, Pindos mountains [48], Vavdos at Chalkidiki [49], Peloponnesus and the Aegean islands [45]. Despite lack of geochemical information from Olympia, where the majority of the helmets were unearthed, Peloponnesus has similar geology with the mainland Greece and it would be expected that chromite minerals be encountered there too. A chemical study of bones from the nearby Hellenistic site of Asine, showed that they had substantial concentrations of Cr, which was attributed to contamination from the soil [50].

Cr_{III} compounds are highly insoluble but they can oxidize to highly soluble Cr_{VI} depending on surrounding ions [51] and the pH of the solution [52]. Adsorption of CrO_4^{2-} increases in acidic conditions on compounds with exposed hydroxyl groups on their surfaces, due to protonation of any hydroxyl compounds and because adsorption is favored by positively charged surfaces at low to neutral pH [53] (p. 316). There is plenty of opportunity for the chromate ion to be adsorbed into the corrosion patina in the burial environment during corrosion. The formation of a metastable $Cu(OH)_2$, the role of which is unclear for the Cu_2O formation, could offer opportunity for chromate adsorption onto OH^- already in the corrosion profile. Analysis showed that measurable Cr with our set-up occurs in samples with Si content greater than about 3 Atomic %. Silicon has high solubility in the aqueous environment and high affinity for oxygen in acidic pH. It is possible that at an early stage, Si^{4+} was adsorbed onto OH^- or O^- present in the corrosion film, in turn facilitating adsorption of the chromate ion as a next step. Si-content is elevated at smooth grey corrosion patinas which in turn is associated with azurite. The role of silicon on the development of stable corrosion films requires further investigation.

Conclusions

Analysis results support and expand current understanding of corrosion mechanisms on low-tin archaeological bronzes. The presence of fibrous or 'tentacle-like' corrosion feature confirms previously reported hypothesis for the complexity of corrosion in the burial [21]. Corrosion profiles that form smooth patinas which preserve polishing marks and act as a marker of the original surface can be developed due to the inward migration of oxygen ions and the *in-situ* oxidation of tin or of copper (in the case where cuprite is formed at the inner zone). The growth of an inner cuprite zone is related to the availability of oxygen and the pH of the solution, as seen in equilibrium Eh/pH diagrams for the Cu-CO_2-H_2O system, with prevailing corrosion mechanisms explaining the formation of azurite or malachite deposits. Kinetics would be important for this, and the role of the $Si^{4+}$to the development of stable patinas requires further investigation. The occurrence of epitactic growth of cuprite and the pseudomorphic preservation of slip lines likely indicates a role for the manufacturing method in the corrosion mechanisms of archaeological bronzes. Further investigation is necessary to elucidate the role of soil elements in the formation and appearance of patinas, with silica seemingly playing an important role.

Funding

This research received funding from Cardiff University PhD Scholarships and COST for the participation at European activities including access to the STFC (previously CCLRC) Daresbury Laboratory.

Data availability statement

The raw/processed data required to reproduce these findings cannot be shared at this time as the data also forms part of an ongoing study.

CRediT authorship contribution statement

Panagiota Manti: Conceptualization, Methodology, Software, Formal analysis, Investigation, Resources, Writing – original draft, Writing – review & editing, Funding acquisition, Project administration. **David Watkinson:** Methodology, Writing – review & editing, Visualization, Project administration.

Acknowledgments

Authors express their gratitude to the Ministry of Greek Culture and the responsible archaeologists to permitting the study, sampling and publishing of the geek helmets. Dr Manolis Pantos is thanked for his encouragement, advice and training on synchrotron based X-ray diffraction; the National Museum of Wales for access to equipment. This work depended on accessing museum collections and excavated helmets from sites in Greece and museums in the UK. Susan Walker, Prof Michael Vickers, Mark Norman, Daniel Bone at the Ashmolean Oxford University Museum; Lucilla Burn, Julie Dawson at the Fitzwilliam Cambridge University Museum; Prof John Prag, Irit Narkiss and Malcolm J. Chapman at the Manchester University Museum; Richard Brewer, Mary Davies and Penny Hill at the National Museum Wales, Cardiff; Birgitte Speake, Gali Beiner, Jeremy Coote, Julia Nicholson, Zena McGreevy at the Pitt Rivers Museum, Oxford. Polixeni Adam-Veleni, Niki Kapizioni, Despoina Ignatiadou, Dimitrios Grammenos, Styliana Galiniki, S. Athanasiadou, A. Papadimitropoulou at the Archaeological Museum of Thessaloniki; Lilian Achilara, Aikaterini Despoini, Vasiliki Misailidou-Despotidou and Dr Konstantinos Sismanidis, for permission to study and publish material from their excavations, from the 16th Ephorate of Prehistoric and Classical Antiquities of Greece (ΙΣΤ' ΕΡΚΑ), Thessaloniki; Maria Akamati, Pavlos Chrisostomou and Anastasia Georgiadou from the 17th Ephorate of Prehistoric and Classical Antiquities of Greece (ΙΖ'ΕΡΚΑ), Pella; Georgia Hatzi-Spiliopoulou, Christos Liagouras, Olga Petropoulou, Christos Anagnostakos from the 7th Ephorate of Prehistoric and Classical Antiquities of Greece (Ζ'ΕΡΚΑ), Olympia Museum; Reinhard Senff and

Susanne Bocher for permitting and facilitating access to material for study and sampling from the German Archaeological Institute at Athens (DAI) and Heide Frielinghaus (from the Institute for Classical Archaeology, University of Regensburg, Germany) for useful communications over selected helmets. Last but not least we are in dept to the reviewers of the original version for their detailed comments and meaningful discussion.

Supplementary materials

Supplementary material associated with this article can be found, in the online version, at doi:10.1016/j.culher.2022.03.004.

References

[1] P.T. Craddock, A. Giumlia-Mair, Beauty is skin deep: evidence for the original appearance of classical statuary, in: P.T. Craddock, S. La Niece (Eds.), Metal Plating and Patination: Cultural, Technical and Historical Developments, Butterworth-Heinemann, Oxford ; Boston, 1993, pp. 30–38.
[2] P.T. Craddock, Scientific investigation of copies, fakes and forgeries, Butterworth-Heinemann (Elsevier), 2009.
[3] R. Hughes, P.T. Craddock, S. La Niece, Artificial patination, in: Metal Plating and Patination: Cultural, Technical and Historical Developments, Butterworth-Heinemann, 1993, pp. 1–18.
[4] R. Bertholon, The location of the original surface, a review of the conservation literature, in: I. MacLeod, J. Theile, C. Degrigny (Eds.), Proceedings of the ICOM Committee for Conservation Metals Working Group, Welshpool, Western Australia, Western Australian Museum, Santiago, Chile, 2001, pp. 167–179. 2-6 April2004.
[5] J. Charbonneaux, Greek Bronzes, Elek Books, London, 1962.
[6] Pausanias, Description of Greece, (n.d.).2022
[7] J. Whitley, Classical art and human agency: a tale of two objects in fifth-century Greece., in: N.C. Stambolidis (ed.), Γενέθλιον: Αναμνηστικός Τόμος Για Την Συμπλήρωση Είκοσι Χρόνων Λειτουργίας Του Μουσείου Κυκλαδικής Τέχνης., N.P. Goulandris Museum, Athens, 2006: pp. 227–236.
[8] L. Robbiola, J.M. Blengino, C. Fiaud, Morphology and mechanisms of formation of natural patinas on archaeological Cu-Sn alloys, Corros. Sci. 40 (1998) 2083–2111, doi:10.1016/S0010-938X(98)00096-1.
[9] P. Piccardo, B. Mille, L. Robbiola, Tin and copper oxides in corroded archaeological bronzes, in: P. Dillmann, G. Beranger, P. Piccardo, H. Matthiesen (Eds.), Corrosion of Metallic Heritage Artefacts - Investigation, Conservation and Prediction for Long-Term Behaviour, Woodhead Publishing for the European Federation of Corrosion and The Institute of Materials, Minerals and Mining, Cambridge, 2007, pp. 239–262.
[10] L. Robbiola, T.T.M. Tran, P. Dubot, O. Majerus, K. Rahmouni, Characterisation of anodic layers on Cu–10Sn bronze (RDE) in aerated NaCl solution, Corros. Sci. 50 (2008) 2205–2215.
[11] L. Robbiola, D. Vilbert, T. Lejars, D. Bourgarit, B. Mille, Characterisation of a buried archaeological bronze from the Celtic tomb No. 1002 of La Fosse Cotheret (Roissy-En-France)., in: Metal 2001. ICOM Committee for Conservation, Metals Working Group, James & James, London, 2001: pp. 237–242.
[12] T. Weisser, D. Leigh, The De-alloying of copper alloys, in: Conservation in Archaeology and the Applied Arts, IIC, London, 1975, pp. 207–214. IIC Congress, Stockholm.
[13] W.A. Oddy, N.D. Meeks, Unusual phenomena in the corrosion of ancient bronzes, in: N.S. Brommelle, G. Thomson (Eds.), Science and Technology in the Service of Conservation, Preprints of the Contributions to the Washington Congress, IIC, London, 1982, pp. 119–124. 3-9 September 1982.
[14] S. Turgoose, R.C. Janaway, B. Scott, Corrosion and structure: modelling the preservation mechanisms, in: Evidence Preserved in Corrosion Products: New Fields in Artifact Studies, UKIC, Leeds, 1983, p. 1989. Proceedings of a Joint Conference Between UKIC Archaeology Section and the Council for British Archaeology Science Committee.
[15] D.A. Scott, Copper and Bronze in Art: Corrosion, Colorants, Conservation, Getty Conservation Institute, L.A., 2002 https://www.getty.edu/conservation/publications_resources/books/copper_bronze_in_art.html.
[16] N.D. Meeks, Tin-rich surfaces on bronze - some experimental and archaeological considerations, Archaeometry 28 (1986) 133–162, doi:10.1111/j.1475-4754.1986.tb00383.x.
[17] S. La Niece, Silvering, P.T. Craddock, S. La Niece, in: Metal Plating and Patination: Cultural, Technical and Historical Developments, Butterworth-Heinemann, Oxford ; Boston, 1993, pp. 201–210.
[18] P. Manti, D. Watkinson, Hot-tinning of low tin bronzes, in: P. Mardikian, C. Chemello, C. Watters, P. Hull (Eds.), Proceedings of the Interim Meeting of the International Council of Museums Committee For Conservation Metal Working Group, Clemson University, Charleston, Charleston, South Carolina, USA, 2011, pp. 92–98. 11-15 October 2010.
[19] P. Manti, D. Watkinson, Examination of Greek bronze helmets: sampling and project design, in: C. Degrigny, R. Van Langh, B. Ankersmit (Eds.), Proceedings of the Metal 07, The ICOM-CC Metal Working Group International Triennial Meeting, ICOM-CC Metals Group, Rijksmuseum-Amsterdam, Rijksmuseum, 2007, pp. 78–82. 17-21 September 2007.
[20] E. Bidaud, D. Benedetti, R. Bugoi, B. Comendador, S. Goidanich, P.C. Gutiérrez, D. Garipoli, P. Manti, T. Mifsud, V. Urbina, W. Kockelmann, A.D. Smith, F. Bahrami, M.A. MacDonald, A.M.T. Bell, P. Rizkallah, R. Jones J., E. Pantos, The COST-G8 master class on SR in cultural heritage at DL-SRS and RAL-ISIS, (2006).
[21] P. Piccardo, M. Mödlinger, G. Ghiara, S. Campodonico, V. Bongiorno, Investigation on a “tentacle-like” corrosion feature on Bronze Age tin-bronze objects, Appl. Phys. A 113 (2013) 1039–1047, doi:10.1007/s00339-013-7732-1.
[22] R.J. Davis, Copper and Copper Alloys (2001).
[23] Italia Meridionale O. Colacicchi-Alessandri, M. Ferretti, V.S.A.C. Indagini Su Manufatti Di Bronzo Del, A. Giumlia-Mair, I. Bronzi Antichi, Provenienti Dalla Necropoli Di Vaglio, in: Produzione e Tecnologia: Atti Del XV Congresso Internazionale Sui Bronzi Antichi Organizzato Dall’Università Di Udine, Sede Di Gorizia, Grado-Aquilieia, Maggio, 2001, pp. 137–142. 22-262002.
[24] M. Pourbaix, Electrochemical corrosion and reduction., in: corrosion and metal artifacts - a dialogue between conservators and archaeologists and, corrosion scientists, National Bureau of Standards, Maryland, 1977: pp. 1–16.
[25] Chapter 2.02 G.T Burstein, R.A. Cottis, J.M. Graham, R. Linsday, S.B. Lyon, J.A. Richardson, F.H. Scott, J.D. Scantlebury, Passivity and localised corrosion, in: Shreir’s Corrosion, 4th ed., Elsevier, Amsterdam, 2010, pp. 731–752.
[26] J.H. Payer, G. Ball, B.I. Rickett, H.S. Kim, Role of transport properties in corrosion product growth, Mater. Sci. Eng. A 198 (1995) 91–102, doi:10.1016/0921-5093(95)80063-Z.
[27] L. Robbiola, N. Pereira, K. Thaury, C. Fiaud, J.P. Labbe, Decuprification phenomenon of Cu-Sn alloys in aqueous solution in nearly neutral pH conditions, in: W. Mourey, L. Robbiola (Eds.), Metal 98. ICOM Committee for Conservation, Metals Working Group, James & James, London, 1998, pp. 136–144.
[28] D.D. Macdonald, M. Urquidi-Macdonald, Theory of steady-state passive films, J. Electrochem. Soc. 137 (1990) 2395–2402, doi:10.1149/1.2086949.
[29] L.F. Lin, C.Y. Chao, D.D. Macdonald, A point defect model for anodic passive films. II. Chemical breakdown and pit initiation, J. Electrochem. Soc. 128 (1981) 1194–1198, doi:10.1149/1.2127592.
[30] Chapter 1 B. Pieraggi, R.A. Cottis, J.M. Graham, R. Linsday, S.B. Lyon, J.A. Richardson, J.D. Scantlebury, et al., Defects and transport in oxides and oxide scales, in: Shreir’s Corrosion, 06, 4th ed., Elsevier, Amsterdam, 2010, pp. 101–131.
[31] E. Sidot, N. Souissi, L. Bousselmi, E. Triki, L. Robbiola, Study of the corrosion behaviour of Cu–10Sn bronze in aerated Na_2SO_4 aqueous solution, Corros. Sci. 48 (2006) 2241–2257, doi:10.1016/j.corsci.2005.08.020.
[32] D. Šatović, L.V. Žulj, V. Desnica, S. Fazinić, S. Martinez, Corrosion evaluation and surface characterization of the corrosion product layer formed on Cu–6Sn bronze in aqueous Na2SO4 solution, Corros. Sci. 51 (2009) 1596–1603, doi:10.1016/j.corsci.2009.04.002.
[33] S.C. Britton, The Corrosion Resistance of Tin and Tin Alloys, Tin Research Institute, Greenford, Middx, 1952.
[34] L. Robbiola, L.P. Hurtel, Standard nature of the passive layers of buried archaeological objects: the example of two roman half-length portraits, in: Metal 95. International Conference on Metals Conservation, James & James, Semur en Auxois, 1997, pp. 109–117. 25-28 Sept. 1995.
[35] I.T. Vargas, P.A. Pastén, G.E. Pizarro, Empirical model for dissolved oxygen depletion during corrosion of drinking water copper pipes, Corros. Sci. 52 (2010) 2250–2257, doi:10.1016/j.corsci.2010.03.009.
[36] K. Krauskopf, D. Bird, Introduction to Geochemistry, 3rd ed., McGraw-Hill International Editions, New York, 1995.
[37] I.T. Vargas, M.A. Alsina, P.A. Pastén, G.E. Pizarro, Influence of solid corrosion by-products on the consumption of dissolved oxygen in copper pipes, Corros. Sci. 51 (2009) 1030–1037, doi:10.1016/j.corsci.2009.02.014.
[38] J. Kunze, V. Maurice, L.H. Klein, H.H. Strehblow, P. Marcus, *In situ* STM study of the duplex passive films formed on Cu(111) and Cu(001) in 0.1M NaOH, Corros. Sci. 46 (2004) 245–264, doi:10.1016/S0010-938X(03)00140-9.
[39] W. Wang, D. Wu, Q. Zhang, L. Wang, M. Tao, pH-dependence of conduction type in cuprous oxide synthesized from solution, J. Appl. Phys. 107 (2010) 123717–4, doi:10.1063/1.3452383.
[40] Chapter 2.01 G.S. Frankel, R.A. Cottis, R.A. Cottis, J.M. Graham, R. Linsday, S.B. Lyon, J.A. Richardson, J.D. Scantlebury, et al., Principles of Corrosion in Liquids, in: Shreir’s Corrosion, 4th ed., Elsevier, Amsterdam, 2010, pp. 725–731.
[41] J.D. Fenn, K. Foley, Passivation of iron, Stud. Conserv. 20 (1975), doi:10.1179/sic.1975.s1.033.
[42] H. Rubin, M. Zhaozeng, W. Zengjun, T. Ko, Studies in the black passive oxide film on bronze arrowheads unearthed with the terra-cotta warriors near the Qin Tomb (210bc) at Lintong, Xian, Stud. Hist. Nat. Sci. 2 (1983) 295–302.
[43] N.D. Meeks, Surface characterization of tinned bronze, high-tin bronze, tinned iron and arsenical bronze, in: Metal Plating and Patination: Cultural, Technical and Historical Developments, Butterworth- Heinemann, Oxford ; Boston, 1993, pp. 247–275.
[44] M. Martinón-Torres, X. Li, Y. Xia, A. Benzonelli, A. Bevan, S. Ma, J. Huang, L. Wang, D. Lan, J. Liu, S. Liu, Z. Zhao, K. Zhao, T. Rehren, Surface chromium on Terracotta Army bronze weapons is neither an ancient anti-rust treatment nor the reason for their good preservation, Sci. Rep. 9 (2019) 5289, doi:10.1038/s41598-019-40613-7.
[45] S. Karavoltsos, A. Sakellari, N. Mihopoulos, M. Dassenakis, M.J. Scoullos, Evaluation of the quality of drinking water in regions of Greece, Desalination 224 (2008) 317–329, doi:10.1016/j.desal.2007.06.013.
[46] Encyclopedia of European and Asian Regional Geology, Kluwer Academic Publishers, Dordrecht, 1997, doi:10.1007/1-4020-4495-X.

[47] S.S.P. Augustithis, Atlas of the Textural Patterns of Ore Minerals and Metallogenic Processes, De Gruyter, 1995, doi:10.1515/9783110895506.
[48] M. Economou-Eliopoulos, I. Vacondios, Geochemistry of chromitites and host rocks from the Pindos ophiolite complex, northwestern Greece, Chem. Geol. 122 (1995) 99–108.
[49] C. Christodoulou, D.M. Hirst, The chemistry of chromite from two mafic—ultramafic complexes in northern Greece, Chem. Geol. 49 (1985) 415–428.
[50] J. Edward, J.M. Fossey, L. Yaffe, Analysis by neutron activation of human bone from the hellenistic cemetery at Asine, Greece, J. Field Archaeol. 11 (1984) 37–46.
[51] L. Reyes-Gutiérrez, E. Romero-Guzmán, A. Cabral-Prieto, R. Rodríguez-Castillo, Characterization of chromium in contaminated soil studied by SEM, EDS, XRD and mössbauer spectroscopy, J. Miner. Mater. Charact. Eng. 7 (2007) 59–70.
[52] Z. Stępniewska, K. Bucior, M. De Boodt, Chromium and its forms in soils in the proximity of the old tannery waste lagoon, Int. Agrophys. 15 (2001) 121–124.
[53] D. Adriano, Trace Elements in the Terrestrial Environment: Biogeochemistry, Bioavailability, and Risks of Metals, 2nd ed., Springer-Verlag, New York, 2001.